A Numerical Study of Circulation in the Western Caribbean Sea

JINYU SHENG AND LIQUN TANG

Department of Oceanography, Dalhousie University, Halifax, Nova Scotia, Canada

(Manuscript received 22 May 2002, in final form 4 April 2003)

ABSTRACT

A three-dimensional ocean circulation model is used to study circulation and month-to-month variability in the western Caribbean Sea. The domain covers the area between 72° and 90°W and between 8° and 24°N, with a horizontal resolution of roughly 18 km. The western Caribbean Sea model is forced by the monthly mean Comprehensive Ocean–Atmosphere Data Set (COADS) wind stress and surface heat flux and monthly mean volume transports through the model open boundaries calculated by a (1/3)° Atlantic Ocean model. The model sea surface salinity is restored to the monthly mean climatology. The semiprognostic method suggested by Sheng et al. is used to reduce the model errors by assimilating the hydrographic data into the momentum equations. The model reproduces many well-known circulation features in the region, including the warm and persistent throughflow known as the Caribbean Current, the highly variable Panama–Colombia Gyre, and moderate seasonal variations of temperature and salinity in the surface mixed layer. The overall features of the model-calculated 10-yr mean near-surface circulation are in good agreement with the decadal-mean currents inferred from the trajectories of the satellite-tracked 15-m drogued drifters by Fratantoni. The vertical distributions of the time-mean model currents across the Yucatan Strait qualitatively agree with the time-mean observed currents made by Sheinbaum et al. The model results demonstrate that nonlinear dynamics play a very important role in simulating month-to-month and mesoscale variability in the western Caribbean, particularly over the southern Colombian Basin and eastern Cayman and Yucatan Basins. The monthly varying wind stress and boundary flows also play an important role in simulating general circulation and variability in the region. The monthly varying surface heat and freshwater fluxes are largely responsible for the seasonal cycle of temperature and salinity in the surface mixed layer.

1. Introduction

The Caribbean Sea (hereinafter CS) is the largest marginal sea of the Atlantic Ocean, separated from the main Atlantic basins by an island-studded enclosure. The CS is connected to the North Atlantic Ocean via the Lesser Antilles and Windward Passages to the east and the Gulf of Mexico via the Yucatan Strait to the north. It consists of a succession of five basins: the Grenada, Venezuelan, Columbian, Cayman, and Yucatan Basins. The CS has a surface extension of about 2.52×10^6 km^2 and volume of about 6.48×10^6 km^3 (Gallegos 1996). Its surface area is roughly twice as large as that of the Gulf of Mexico. Its volume is roughly twice as large as that of the Mediterranean Sea. The highly variable bottom topography and remarkably irregular coastline of the CS significantly affect the physical processes at work in the region.

The CS waters are highly stratified in the upper 1200 m, weakly stratified between 1200 and 2000 m, and nearly homogeneous below 2000 m (Wust 1964). Water temperature in the top mixed layer has moderate seasonal variations. The CS surface waters are also affected by freshwater runoff from three major rivers known as the Magdalena, Orinoco, and Amazon Rivers, the annual mean discharges of which are about 7.5×10^3, 3.9×10^4, and 1.7×10^5 m^3 s^{-1}, respectively (Muller-Karger 1993; Mooers and Maul 1998). The Magdalena River discharges directly into the CS and interacts with the circulation in the southwestern CS. The Orinoco River plume flows first northward along the South American coast and then influences the islands of the southern Lesser Antilles. During the high runoff period, a significant amount of the Orinoco estuarine waters enter the southern CS through the southernmost passages of the Antilles and continue on the west-northwestward drift. The Amazon River plume influences the CS mainly during boreal winter and spring. In summer and fall, much of the Amazon River plume flows offshore toward Africa, playing a lesser role in driving the circulation in the CS.

The CS is under the influence of the southwestern quadrant of the North Atlantic trade winds, which are geostrophically balanced and well established in summer (Mooers and Maul 1998). As a result, the average winds over the Caribbean region are persistent both in direction and magnitude (3.5–10.5 m s^{-1}; Gallegos

Corresponding author address: Dr. Jinyu Sheng, Department of Oceanography, Dalhousie University, Halifax NS B3H 4J1, Canada. E-mail: jinyu.sheng@dal.ca

1996). On average, easterly or northeasterly winds prevail over the region in winter and easterly or southeasterly winds prevail in summer. Frequent interruptions to the trade winds are the tropical storms and hurricanes in summer and autumn and weekly eastward cold-front passages over the northern CS in winter.

General circulation and water mass distributions in the CS have been studied for more than a hundred years (Wust 1964; Gordon 1967; Worthington 1976; Roemmich 1981; Gallegos 1996; Murphy et al. 1999; Johns et al. 2002). A reader is referred to Kinder et al. (1985), Maul (1993), and Mooers and Maul (1998) for comprehensive overviews of the regional oceanography in the region. The upper-ocean circulation in the CS is dominated by a warm and persistent throughflow known as the Caribbean Current. The Caribbean Current flows westward about 200–300 km off the northern coast of South America and then northward along the eastern coast of Central America. It becomes known as the Yucatan Current as it flows through the Yucatan Channel and then becomes known as the Loop Current as it penetrates northward in the eastern Gulf of Mexico (Mooers and Maul 1998). The other important circulation features include the highly variable Panama–Columbia Gyre in the southwestern CS, where it interacts with the estuarine plume of the Magdalena River.

The main objective of this paper is to examine the ocean circulation and temperature–salinity distributions and their seasonal and month-to-month variability in the western Caribbean Sea (WCS) using a three-dimensional primitive equation ocean circulation model. Our study is motivated by an increasing demand for protecting marine ecosystems in the CS. The shallow-water tropical ecosystems that consist of coral reefs, mangroves, estuaries, and seagrass beds are major natural resources in the region. These unique marine ecosystems have been significantly affected by natural and anthropogenic activities such as eutrophication of coastal waters, excessive terrestrial runoff, and sedimentation from deforestation. The ocean circulation model presented in this paper will be used to develop a high-resolution coupled physical–biological modeling system for the Meso-American Barrier Reef System (MBRS) from the Bay Islands of Honduras to the southern half of the Yucatan Peninsula. This coupled modeling system will then be used to study the ecological connections among reefs in the MBRS.

Various numerical methods and models have been applied to the CS in the past. Gordon (1967) and Roemmich (1981) estimated the large-scale circulation from observed hydrographic data in the CS using the geostrophic method and inverse method respectively. Kinder et al. (1985) used a reduced-gravity ocean model to study the formation and propagation of mesoscale eddies in the upper ocean of the southeastern Caribbean Sea. Hurlburt and Townsend (1994) applied the Naval Research Laboratory layered ocean model (NLOM) to the CS and the Gulf of Mexico. Mooers and Maul (1998) applied the terrain-following Princeton Ocean Model to the Intra-Americas Sea (IAS) and forced the model with the monthly mean wind stress developed by Hellerman and Rosenstein (1983) and volume transports across the model open boundaries. Their model results reproduce many major features of the general circulation and mesoscale variability in the IAS. Murphy et al. (1999) recently applied the NLOM to the IAS and examined the connectivity of the CS eddies with the Atlantic Ocean and the Gulf of Mexico. They forced the NLOM using the daily European Centre for Medium-Range Weather Forecasts (ECMWF) winds and boundary flows, with the model density relaxed to annual mean climatological density. Their model results demonstrate the dominant role of the mesoscale eddies in the geostrophically balanced surface layer variability of the CS circulation and connectivity between the North Brazil Current and eddy generation in the eastern Caribbean. Most recently, Johns et al. (2002) applied the NLOM to the Atlantic Ocean from 20°S to 65°N and forced the model with Hellerman and Rosentein's monthly mean wind and volume transports through the southern and northern model open boundaries. In this study, a three-dimensional primitive equation *z*-level ocean model is applied to the WCS with a horizontal resolution of about 18 km. In addition, the semiprognostic method suggested by Sheng et al. (2001) is used to reduce the model drift. The limited-area WCS ocean circulation model, together with the semiprognostic method, is used to examine the response of the western Caribbean Sea to the local wind stress, sea surface heat and salinity fluxes, and remotely generated flows that enter the study region through the Windward Islands Passages.

The arrangement of this paper is as follows. The next section introduces the ocean model and semiprognostic method. Section 3 discusses the monthly mean climatology used to drive the model. Section 4 presents the model results and section 5 presents the model sensitivity studies. The final section is a summary and conclusions.

2. The ocean circulation model and semiprognostic method

The ocean circulation model used in this study is the three-dimensional primitive equation *z*-level ocean model known as CANDIE (Canadian version of DieCAST; Sheng et al. 1998). It is an outgrowth of the DieCAST model developed by Dietrich et al. (1987). CANDIE has been subjected to rigorous testing (D. Wright 2002, personal communication) and successfully applied to various modeling problems on the shelf, including wind-driven circulation over an idealized coastal canyon (Sheng et al. 1998), a density-driven coastal current (Sheng 2001), tidal circulation in the Gulf of St. Lawrence (Lu et al. 2001), and wind-driven circulation over a stratified coastal embayment (Davidson et al. 2001). Most recently CANDIE has been applied to

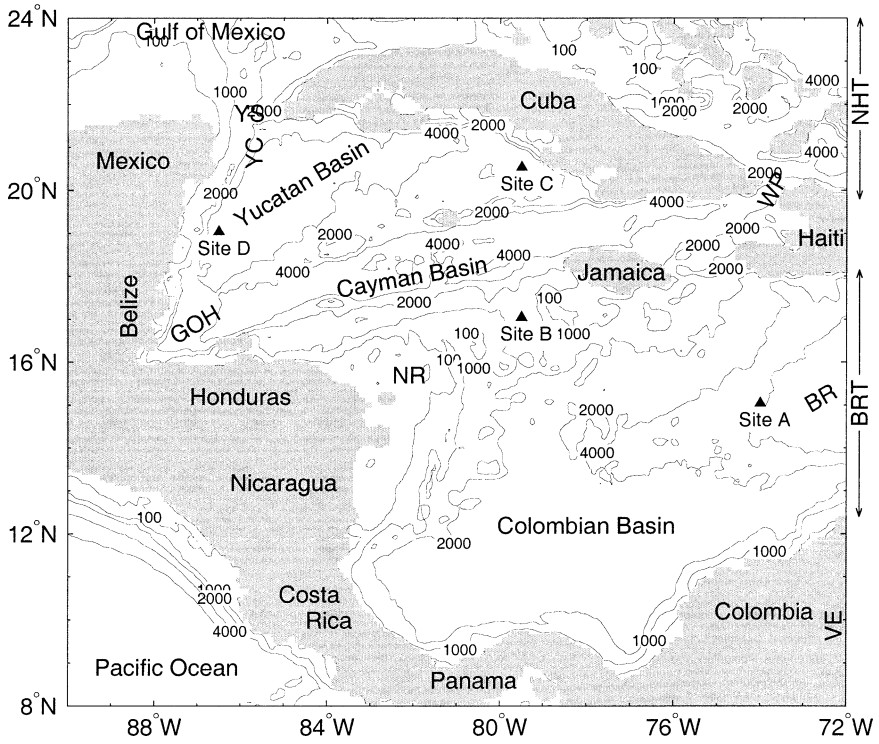

FIG. 1. Selected bathymetric features within the model domain of the western Caribbean Sea model. Abbreviations are used for the northern Haiti Transect (NHT), Windward Passage (WP), Beata Ridge Transect (BRT), Venezuela (VE), Beata Ridge (BR), Yucatan Channel (YC), Yucatan Strait (YS), Gulf of Honduras (GOH), and Nicaragua Rise (NR). Contours are labeled in meters. The four sites marked by solid triangles are chosen to present model results.

the northwestern Atlantic Ocean from northern Labrador to Maine by Sheng et al. (2001). The reader is referred to the appendix for governing equations and subgrid-scale mixing parameterizations used in CANDIE.

The model covers the WCS between 72° and 90°W and between 8° and 24°N (Fig. 1) using the ETOPO5 bathymetry, a gridded elevation/bathymetry for the world complied by the U.S. National Geophysical Data Center, National Oceanic and Atmospheric Administration. The model resolution is one-sixth of a degree in longitude (about 18 km), with the grid spacing in latitude chosen so that, when measured in kilometers, the grid spacing in the northward and eastward directions remains equal at all latitudes. There are 31 unevenly spaced z levels with the centers of each level located at 5, 16, 29, 44, 61, 80, 102, 128, 157, 191, 229, 273, 324, 383, 450, 527, 615, 717, 833, 967, 1121, 1297, 1500, 1733, 2000, 2307, 2659, 3063, 3528, 4061, and 4673 m, respectively.

The WCS model in the control run is initialized with the January mean climatological temperature and salinity fields and forced by monthly mean surface wind stress and heat flux, and flows through the model open boundaries. The net heat flux through the sea surface (Q_{net}) is expressed as (da Silva et al. 1994)

$$Q_{\text{net}} = Q_{\text{net}}^{\text{clim}} + \beta(\text{SST}^{\text{clim}} - \text{SST}^{\text{model}}), \qquad (1)$$

where $Q_{\text{net}}^{\text{clim}}$ is the monthly mean Comprehensive Ocean–Atmosphere Data Set (COADS) net heat flux interpolated onto the model grid and taken from da Silva et al. (1994) and β is the coupling coefficient defined as $\Delta z_1 \rho_o c_p/\tau_Q$, where Δz_1 is the thickness of the top z level, c_p is the specific heat, and τ_Q is the restoring timescale, which is set to 15 days. The implied value of β is about 35 W m^{-2} K^{-1}, which is comparable to values calculated from observations (e.g., Haney 1971). The salinity in the top 10 m is restored to monthly mean climatology with a timescale of 15 days.

At the model lateral closed boundaries, the normal flow, tangential stress of the currents and horizontal fluxes of temperature and salinity are set to zero (free-slip conditions). Along the model open boundaries, the normal flow, temperature, and salinity fields are calculated using the method similar to the adaptive open boundary conditions suggested by Marchesiello et al. (2001). It first uses an explicit Orlanski radiation condition (Orlanski 1976) to determine whether the open boundary is passive (outward propagation) or active (inward propagation). If the open boundary is passive, the model prognostic variables are radiated outward to allow any perturbation generated inside the model domain to propagate outward as freely as possible. If the open boundary is active, the model prognostic variables

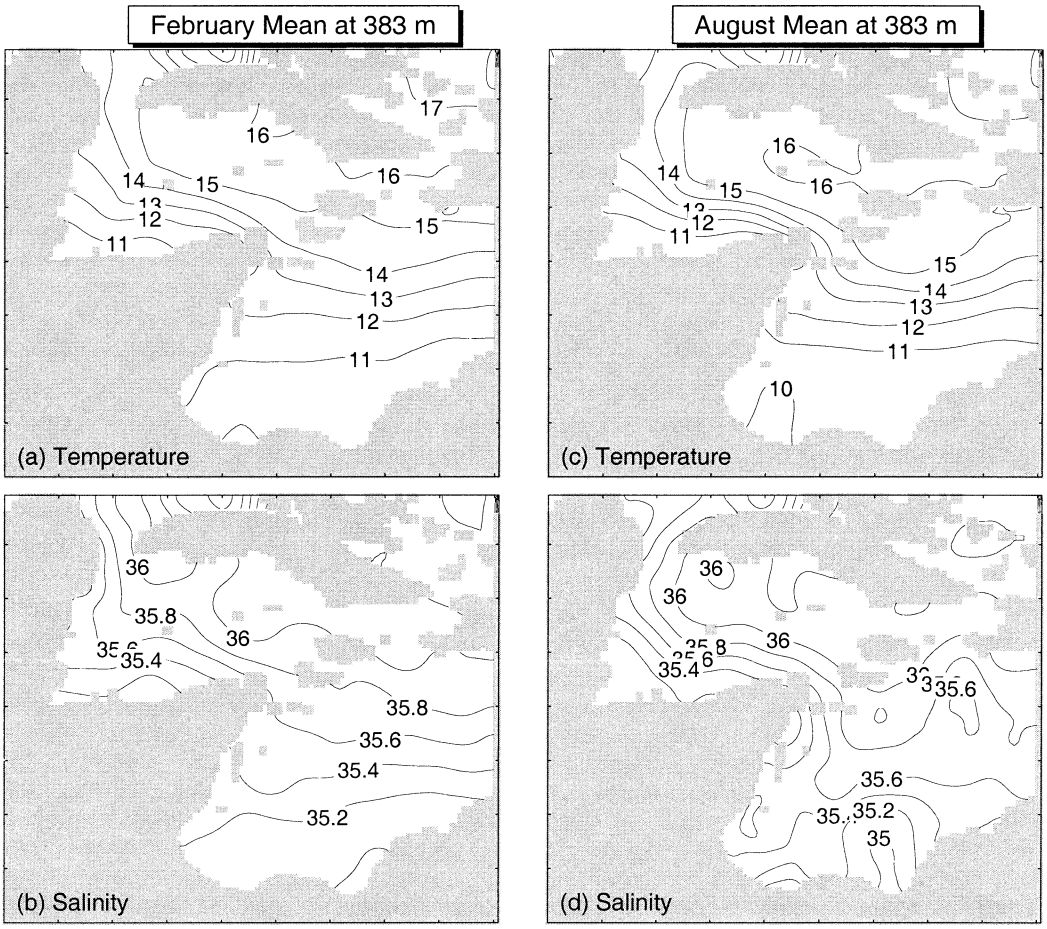

FIG. 2. Climatological monthly mean temperature and salinity at 383 m in the western Caribbean Sea in (a), (b) Feb and (c), (d) Aug, gridded from the hydrographic data compiled by the NODC using the Barnes algorithm.

at the open boundary are restored to the monthly mean climatologies at each z level with the timescale of 15 days. Furthermore, the depth-mean normal flow across the model open boundaries are set to be the monthly mean results produced by a (1/3)° Atlantic model to be discussed in section 3.

To reduce model drift, the semiprognostic method suggested by Sheng et al. (2001) is used in this study. It is a method to adiabatically adjust the momentum equations of an ocean circulation model to correct for the model errors associated with the physical processes that are not correctly represented by the model equations. The adjustment is accomplished by replacing the density term in the hydrostatic equation by a linear combination of model-computed (ρ_m) and climatological (ρ_c) density: $\alpha\rho_m + (1 - \alpha)\rho_c$, where α is a linear combination coefficient [Eq. (A4) in the appendix]. The procedure corresponds to adding a forcing term to the momentum equation through the computation of the horizontal pressure gradient terms. The method is hence adiabatic, leaving the temperature and salinity equations unconstrained and fully prognostic. The reader is referred to Sheng et al. (2001) for the choice of α. In this paper, we follow them and set α to 0.5.

3. Monthly mean hydrography and model forcing

The monthly mean climatologies of temperature and salinity were gridded from the hydrographic data compiled at the National Oceanographic Data Center (NODC) using the Barnes algorithm. Barnes's algorithm is one of the more effective successive-correction methods used for example in mesoscale analysis of radar and satellite data. As the number of iterations increases the interpolated values approach the observations (Daley 1991).

The subsurface waters at 383 m in February and August (Fig. 2) are characterized as relatively cold and fresh over the southwestern CS off Panama and Colombia, warm and salty over the shelf seas off Cuba, and large temperature and salinity gradients along the pathway of the Caribbean Current that flows from the northern Colombian to the western Cayman and Yucatan Basins. Furthermore, the upper-ocean salinity in August

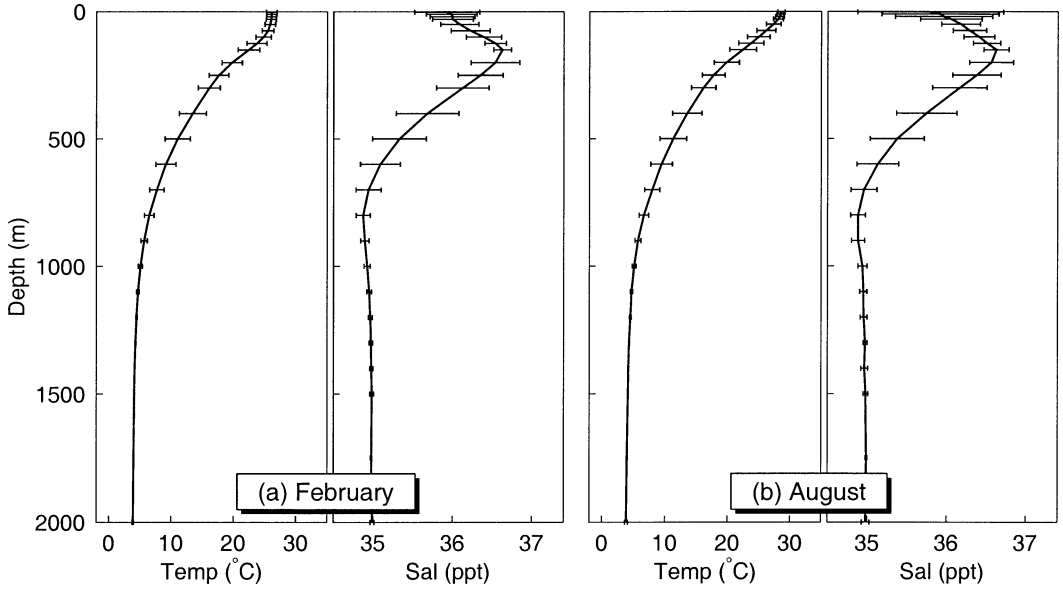

FIG. 3. Vertical profiles of the domain-averaged climatological monthly mean temperature and salinity (gridded from the hydrographic data compiled by the NODC using the Barnes algorithm) and the rms values with respect to the domain means at each depth in the western Caribbean in (a) Feb and (b) Aug. The length of the error bar represents 2 std dev.

has larger horizontal variations than in February, due mainly to larger freshwater discharges from the Magdalena River in summer and autumn than in the other two seasons.

The water column in the region, on average, can be described as a four-layer system (Fig. 3): a warm and relatively fresh surface mixed layer of less than 100-m depth, a relatively warm and salty subsurface layer centered at roughly 200 m, a relatively cold and fresh intermediate layer centered at roughly 700 m, and a nearly homogeneous deep layer below 2000 m (Gallegos 1996; Mooers and Maul 1998). To quantify horizontal variations of gridded monthly mean hydrography in the WCS, we calculate the domain-averaged temperature and salinity and associated root-mean-square (rms) deviations with respect to the domain means at each z level. A large rms value represents large spatial variability. Horizontal variations of the monthly mean temperature in the top 100 m are small in February and August (Fig. 3). By contrast, the monthly mean salinity has relatively large horizontal variations in the surface mixed layer, associated primarily with river discharges. The monthly mean temperature and salinity in the subsurface and intermediate layers between 100 and 1000 m have relatively large horizontal variations. In the deep layer of greater than 1500 m, the monthly mean temperature and salinity are nearly homogeneous horizontally.

Two types of forcings are used to drive the model in this study. The first type is the climatological monthly mean wind stress, and sea surface heat and freshwater fluxes. The second type is the monthly mean volume transport through Windward Islands Passages.

The climatological monthly mean COADS surface wind stress and net heat flux with a 0.5° resolution (da Silva et al. 1994) are used in this study. The monthly mean wind forcing in the region is characterized by the persistent southwestward wind stress in the Colombian Basin and relatively weak (Fig. 4), roughly westward wind stress over the Cayman and Yucatan Basins. The wind stress in the western Caribbean, on average, is relatively stronger in winter months and weaker from August to October.

Surface heat fluxes over the WCS are negative (i.e., the ocean waters losing heat to the atmosphere) from November to January, with larger heat losses in the Cayman and Yucatan Basins than those in the Colombian Basin. From April to September, the heat fluxes are positive in the WCS, with relatively large heat gains over the coastal area off Colombia in spring and summer, and Yucatan and Cayman Basins from later spring to early summer. The surface heat fluxes in February are negative over the western Caribbean, except for the coastal areas of Panama and Colombia.

The WCS model has the eastern open boundary at 72°W, comprising two meridional transects: (a) the Beata Ridge Transect between Haiti and Colombia and (b) the northern Haiti Transect (Fig. 1). The depth-mean flows through these two transects are specified based on the monthly mean volume transport produced by a (1/3)° ocean circulation model for the Atlantic Ocean using the Family of Linked Atlantic Model Experiments (FLAME; Dengg et al. 1999). The total volume transport through the Windward Passage and Beata Ridge Transect is roughly equal to the total transport through the island arc known as the Windward Islands Passages

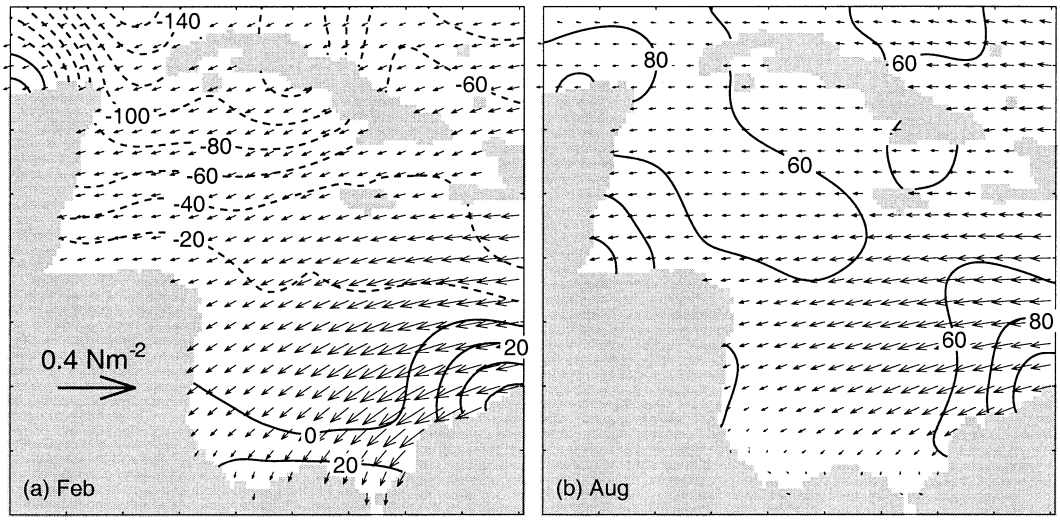

FIG. 4. Climatological monthly mean COADS surface wind stress vectors and heat fluxes in (a) Feb and (b) Aug. Positive heat fluxes mean ocean waters gain heat from the atmosphere. Contour intervals are 10 W m^{-2}.

from Cuba to Trinidad. For the depth-mean boundary flow across the northern Haiti Transect, on the other hand, only the portion of the transport that enters through the Windward Passage between Haiti and Cuba affects the circulation in the WCS.

Considerable studies have been made in the past to determine the mean volume transport through the Windward Islands Passages. Table 1 lists widely cited estimates of the time-mean transports through three transects in the region: the Southern Windward Islands Passages (SWIP) between Haiti and Trinidad, Windward Passage (WP), and Yucatan Strait (YS). The reader is referred to Johns et al. (2002) for the latest review of the various estimates. Based on the current-meter observations and numerical modeling experiments, Johns et al. (2002) suggested that the time-mean transport is about 18.4 Sv (1 Sv = 10^6 m^3 s^{-1}) for the SWIP and 7.4 Sv for the WP. In comparison, the time-mean transport calculated by the FLAME is about 14.5 Sv for the Beata Ridge Transect and 3.1 Sv for the Windward Passage. As a result, the depth-mean flow at the eastern boundary in this study is the superposition of the FLAME monthly mean results and a uniform westward flow of 0.2 cm s^{-1}. The sensitivity of the model results to the depth-mean flow specified at the eastern boundary is discussed in section 5.

Sheinbaum et al. (2002) recently suggested the time mean volume transport across the Yucatan Strait to be only about 23.8 $\pm$ 1 Sv (with 95% confidence interval), which is about 10% smaller than other studies, Sheinbaum et al.'s estimate was based on the 10-month mean observations made by 33 moored current meters and eight bottom-mounted acoustic Doppler current profilers (ADCP) deployed across the strait from September 1999 to June 2000. Although their measurements were the most continuous and high-resolution observations made in the strait, it is not clear whether their low transport estimate across the strait reflects the interannual variability of the Yucatan Current, or indicates the systemic overestimation of the transport across the strait made in the previous studies. In this study, therefore, we follow Johns et al. (2002) and consider the mean volume transport across the Yucatan Strait to be about 26 Sv.

4. Model results

a. Time-mean circulation

We initialize the WCS model with January mean temperature and salinity and force the model with monthly mean wind stress, boundary transport, and surface heat and freshwater fluxes (control run; see Table 2). We integrate the model for 11 yr and calculate the time-mean volume transport streamfunction from the model results during the last 10 yr. The 10-yr mean circulation (Fig. 5a) is characterized by a persistent throughflow associated with the Caribbean Current in the northern Colombian Basin and western Cayman and Yucatan Basins, and a cyclonic recirculation associated with the Panama–Colombia Gyre in the southwestern CS. The large-scale features of the mean transport streamfunction produced by the model compare very well with the numerical results produced by Smith et al. (2000) and Johns et al. (2002) for the WCS region. The time-mean transport of the Caribbean Current is about 19 Sv over the eastern Colombian Basin, and increases gradually up to 23 Sv as flowing onto the western Yucatan Basin. The westward flow through the Windward Passage has a time-mean transport of about 7 Sv. The northward transport through the Yucatan Strait is about 26 Sv. All of the above mean transport values are consistent with the current knowledge of the mean transport in the region (Table 1; see also Murphy et al. 1999; Johns et al. 2002).

TABLE 1. Time-mean volume transport estimates (Sv) through the Southern Windward Islands Passages (SWIP), Windward Passage (WP), and Yucatan Strait (YS). For other estimates, the reader is referred to the reviews made by Kinder et al. (1985) and Johns et al. (2002).

Source	SWIP	WP	YS	Methods
Model (1950)	27.2	0.8	31	Estimated from current measurements
Worthington (1976)	20	10	30	Defant's dynamic method
Gordon (1967)	26–33	<5	31	Geostrophic calculation
Roemmich (1981)	22	7	29	Inverse method
Wunsch and Grant (1982)	20	9	29	Inverse method
Schmitz and Richardson (1991)	22	6.8	28.8	Estimated from current and temperature measurements
Hurlburt and Townsend (1994)	24.3	2.7	26.6	Numerical modeling
Johns et al. (2002)	18.4	7.4	28.4	Estimated from current measurements
Sheinbaum et al. (2002)			23.8	Estimated from current measurements

To demonstrate the importance of baroclinicity in the region, we run the model with horizontally and vertically uniform temperature and salinity (i.e., barotropic run). We force this barotropic model by the monthly varying wind stress and boundary flows only. We integrate the model for 11 yr and calculate the time mean transport streamfunction from the last 10-yr model results (Fig. 5b). Except for the values over the areas adjacent to the model open boundaries where the results are affected strongly by the boundary conditions, the mean transport streamfunction in the barotropic run follows the bathymetry much more closely than that in the control run (Figs. 5a,b). It can be concluded, therefore, that the baroclinicity plays a very important role in driving the general circulation in the WCS.

We now return to the model results in the control run. The 10-yr mean near-surface circulation (Fig. 6) is dominated by the Caribbean Current flowing from the eastern Colombian to the western Yucatan Basin and the cyclonic Panama–Colombia Gyre in the southwestern CS. In the central and eastern Colombia Basin, the near-surface currents are relatively broad and almost westward. The westward currents bifurcate before reaching Nicaragua Rise, with one small branch veering southwestward to form the Panama–Colombia Gyre. The main branch turns northwestward and flows along the outer flank of Nicaragua Rise to form a narrow offshore flow running westward. This offshore flow then turns northward as it approaches the Gulf of Honduras and forms a very strong coastal jet running northward along the east coast of Belize and Mexico. The northward current through the western Yucatan Channel known as the Yucatan Current is highly energetic, with a maximum near-surface speed of about 170 cm s^{-1}.

TABLE 2. List of six numerical experiments driven by different combinations of annual mean (AM) and monthly mean (MM) forcing; CR stands for control run.

Name of run	Wind stress	Model's external forcing		
		Boundary flows	Heat flux	Freshwater flux
CR	MM	MM	MM	MM
AMF	AM	AM	AM	AM
MWS	MM	AM	AM	AM
MBT	AM	MM	AM	AM
MHF	AM	AM	MM	AM
MSF	AM	AM	AM	MM

To examine the model performance, we compare the 10-yr mean near-surface currents produced by the model with the decadal mean currents inferred from the observed trajectories of near-surface drifters by Fratantoni (2001) in the WCS. Based on roughly 1500 trajectories of satellite-tracked, 15-m drogued drifters in the North Atlantic Ocean from January 1990 to December 1999, Fratantoni (2001) constructed a decadal mean near-surface current field in the North Atlantic Ocean on a 1° grid. The 10-yr mean near-surface currents produced by the model are in good agreement with the drifter-derived currents in the WCS, particularly the speeds and directions of the Caribbean Current over the northern Colombian Basin and western Cayman and Yucatan Basins (Fig. 6). In the eastern sides of the two basins, both the model-calculated and drifter-derived near-surface currents are relatively weak. The model results in the southwestern CS also agree qualitatively with the drifter-derived currents, although the drifter-derived Panama–Colombia gyre has a relatively larger cell than the one produced by the model.

Sheinbaum et al. (2002) recently deployed eight moorings across the Yucatan Strait from August 1999 to June 2000. Their moorings comprised 33 current meters and eight bottom-mounted ADCPs. The basic structure of the 10-month mean observed currents consists of the surface-intensified Yucatan Current flowing into the Gulf of Mexico from the CS in the upper layer, weak Yucatan Countercurrent flowing southward beneath it over the western side of the strait, and southward flows at the surface and at depth on the Cuban side (Fig. 7a). The mean observed temperature has the upward curvature of the isotherms in the top 500 m associated with the northward Yucatan Current in the Mexican side and southward countercurrent in the Cuban side (Fig. 7b). The change in curvature of the isotherms in the deep layer of greater than 600 m is associated with the Yucatan Countercurrents in the western side and Cuban Countercurrent in the eastern side (Sheinbaum et al. 2002). The vertical distributions of the model-calculated time-mean along-channel currents (Fig. 7c) and tem-

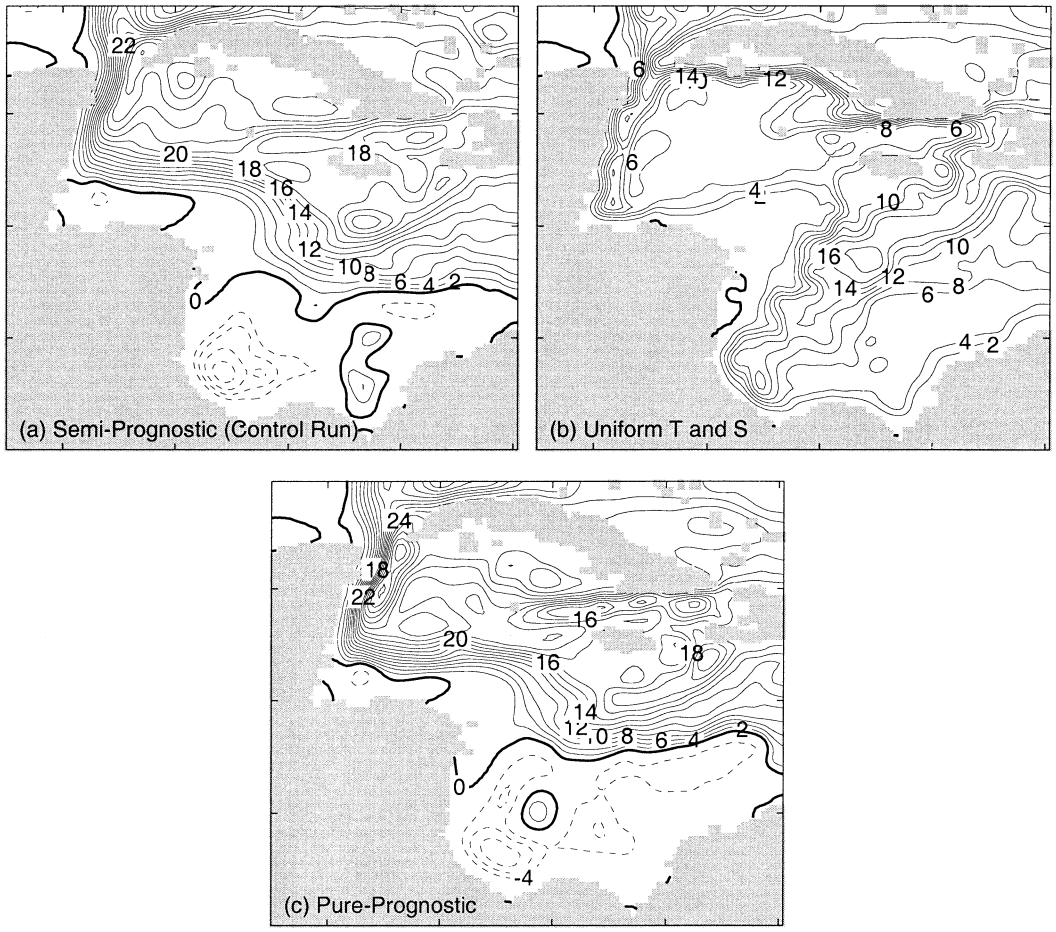

FIG. 5. Mean volume transport streamfunctions (Sv) calculated from 10-yr model results. Contour intervals are 2 Sv. (a) The model is initialized by the Jan mean temperature and salinity and is forced by monthly varying wind stress, boundary flows, and surface heat and freshwater fluxes using the semiprognostic method with $\alpha = 0.5$ (semiprognostic run). (b) The model is initialized with uniform temperature and salinity that remain unchanged in time and is forced by monthly varying wind stress and boundary flows only (barotropic run). (c) The model is initialized and forced in the same way as in (a), but for $\alpha = 1$ (pure-prognostic run).

perature across the strait (Fig. 7d) are in qualitative agreement with the observations made by Sheinbaum et al. It should be noted that the model-calculated Yucatan Current is relatively stronger in the surface layer and the model-calculated Yucatan Countercurrent is relatively weaker than the observations made by Sheinbaum et al. on the western side of the strait.

b. Monthly mean circulation

We also calculate the monthly mean currents and temperature/salinity from the 10-yr model results of the control run. Figure 8 shows the comparison of the model-calculated and climatological monthly mean temperature at five z levels at the four sites marked in Fig. 1. The model results agree reasonably well with the monthly mean climatology in the top 100 m at these four sites, indicating that the WCS model reproduces reasonably well the seasonal cycle of temperature in the region.

The monthly mean near-surface currents at 5 m in February and August have the overall circulation features similar to the time mean near-surface circulation, with the Caribbean Current flowing from the eastern Colombian Basin to the western side of the Yucatan Channel and the Panama–Colombia Gyre over the southwestern CS (Figs. 9a,d). The Caribbean Current is relatively weaker in February than in August. The Panama–Colombia Gyre in February is made up of an intense cyclone over the shelf waters off Costa Rica and Panama. In comparison, the Panama–Colombia Gyre in August is made up of several cyclones of similar size embedded in a larger but weaker cyclonic circulation over the southwestern CS. The highly variable Panama–Colombia Gyre produced by the model qualitatively agrees with the previous findings based on the satellite altimetry data (Nystuen and Andrade 1993; Andrade and Barton 2000) and near-surface drifter data (Fratantoni 2001).

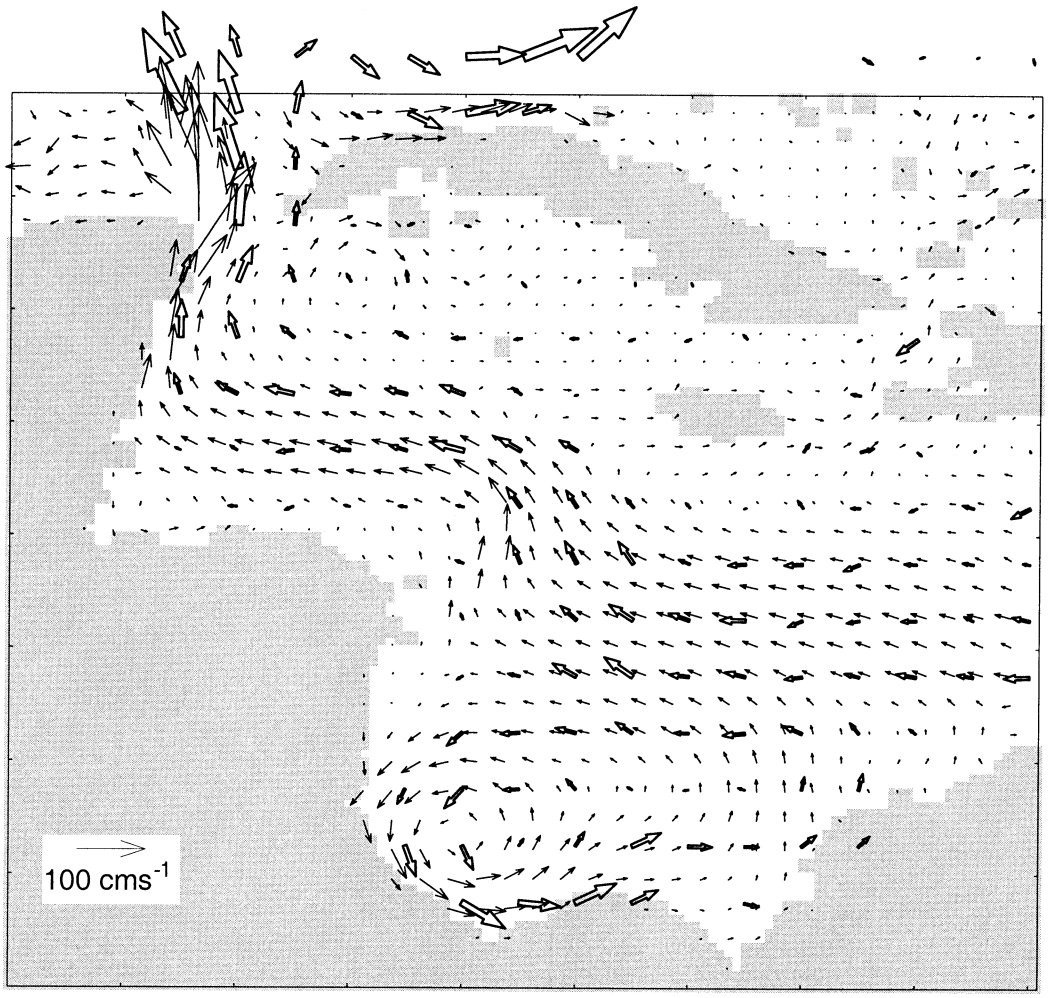

FIG. 6. Comparison of modeled (solid arrows) and observed (open arrows) near-surface currents. The modeled currents are the mean currents at the second top z level centered at 16 m computed from the 10-yr model results. The observed currents are the gridded decadal-mean near-surface currents during the 1990s inferred from trajectories of 15-m drogued satellite-tracked drifters by Fratantoni (2001) on a 1° grid.

The monthly mean near-surface temperature in February and August is horizontally uniform in the CS and about 26°C in February and 28°C in August (Figs. 9b,e). There is a pool of cold waters in the surface layer over the Campeche Bank off northern Mexico. This pool of cold waters is associated with the intense coastal upwelling occurring in the area (Ruiz Renteria 1979). The monthly mean near-surface salinity in both months is horizontally uniform in the central WCS, with relatively salty waters in the eastern Cayman and Yucatan Basins and fresh waters in the southern Yucatan Basin. There is a larger amount of low-salinity waters trapped over the coastal areas off Panama and Colombia in August than in February (Figs. 9c,f).

The monthly mean subsurface circulation at 383 m in February and August (Figs. 10a,d) has large-scale features similar to the time-mean subsurface circulation. Small-scale features over the Colombian Basin and Yucatan Channel are considerably different in these 2 months. The subsurface temperature and salinity at 383 m also have large seasonal variability, with relatively stronger cross-shelf gradients over the western sides of Cayman and Yucatan Basins in August than those in February (Figs. 10b,e and 10c,f). In comparison with the climatology shown in Fig. 2, the model results maintain reasonably well the horizontal gradients of the subsurface temperature and salinity in the region, particularly over the western Cayman and Yucatan Basins.

c. Month-to-month and mesoscale variability

The WCS model generates not only large seasonal variability discussed above, but also substantial month-to-month and mesoscale variability in the region. The model calculated subsurface currents and temperature at 80 m (Fig. 11) exhibit several mesoscale eddies in

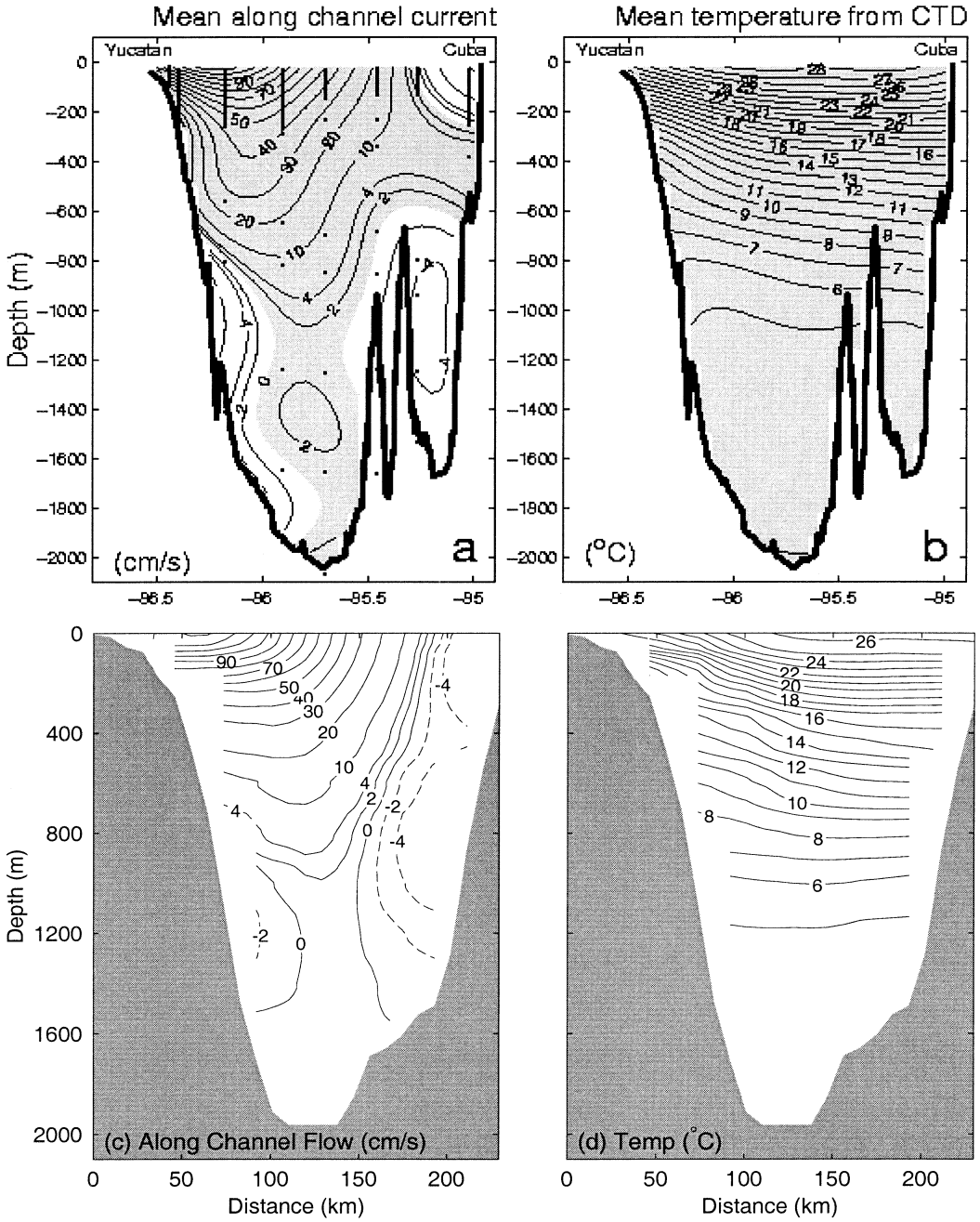

FIG. 7. Time-mean observed (a) currents and (b) temperature across the Yucatan Strait from Aug 1999 to Jun 2000 (adapted from Sheinbuam et al. 2002), and the time-mean (c) currents and (d) temperature across the strait produced by the model.

the WCS during the period from day 660 to 710 (30 October–20 December of the second model year). There are two cyclonic eddies embedded in a large cyclonic recirculation over the southwestern CS around day 660, with two smaller-sized anticyclonic eddies to the southeast. Water temperatures are relatively colder inside the cyclones and warmer inside the anticyclones, as expected. The warm-core anticyclone near the coast of Panama gradually translates northwestward, separating the two cold-core cyclones around day 700. The westward Caribbean Current over the northern Colombian Basin is relatively broad and dynamically steady. Over the eastern Cayman and Yucatan basins, however, there are two intense warm-core anticyclones, both of which translate gradually northwestward to the Yucatan Strait.

To quantify the month-to-month and mesoscale var-

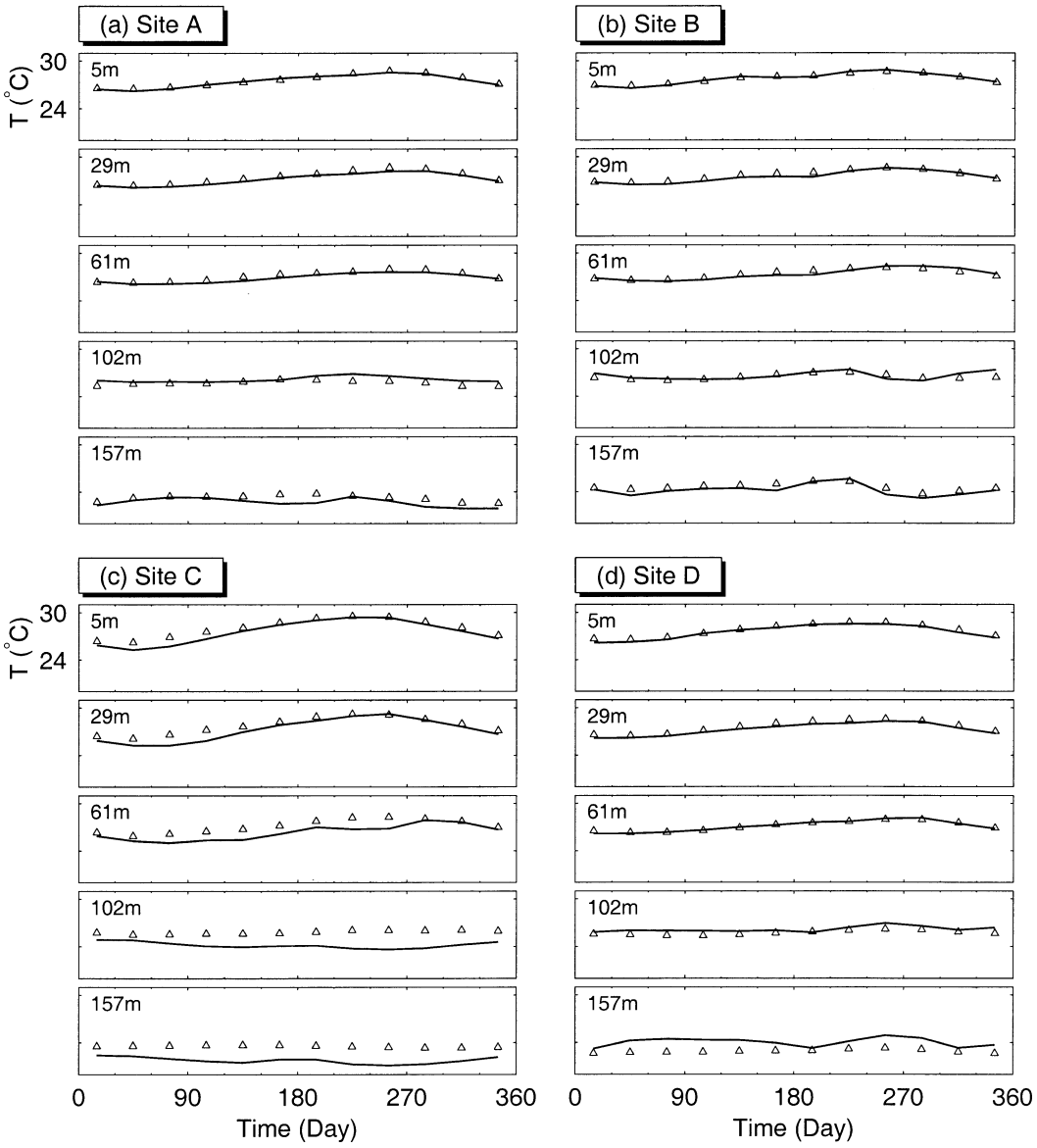

FIG. 8. Comparison of climatological (triangles) and model-computed (solid lines) monthly mean temperature at the upper five z levels at the four sites shown in Fig. 1.

iability of the model results, we examine the root-mean-square values of σ_e and σ_s at each model grid point from the second-year model results. Here σ_e is defined as the rms value of the model results with respect to the monthly mean and σ_s as the rms value of the monthly mean results with respect to the annual mean. We use σ_e to measure the mesoscale variability with timescales of less than 30 days and use σ_s to measure the month-to-month variability with timescales of greater than 30 days. Taking the eastward component of the flow as an example, we have

$$\sigma_e^u = \left[\frac{1}{t_2 - t_1}\int_{t_1}^{t_2} (u - U_m)^2\, dt\right]^{1/2} \quad \text{and} \quad (2)$$

$$\sigma_s^u = \left[\frac{1}{t_2 - t_1}\int_{t_1}^{t_2} (U_m - U_a)^2\, dt\right]^{1/2} \equiv \left[\frac{1}{12}\sum_{m=1}^{12} (U_m - U_a)^2\right]^{1/2}, \quad (3)$$

where U_m ($m = 1, 2, \ldots, 12$) and U_a ($=1/12\ \Sigma_{m=1}^{m=12} U_m$) are the monthly mean and annual mean values of u respectively, and t_1 and t_2 are set to model day 360 and 720, separately.

We divide the WCS into the upper ocean (less than 90 m) and the lower ocean (greater than 90 m) and calculate the vertically averaged rms values in the upper and lower oceans separately, according to

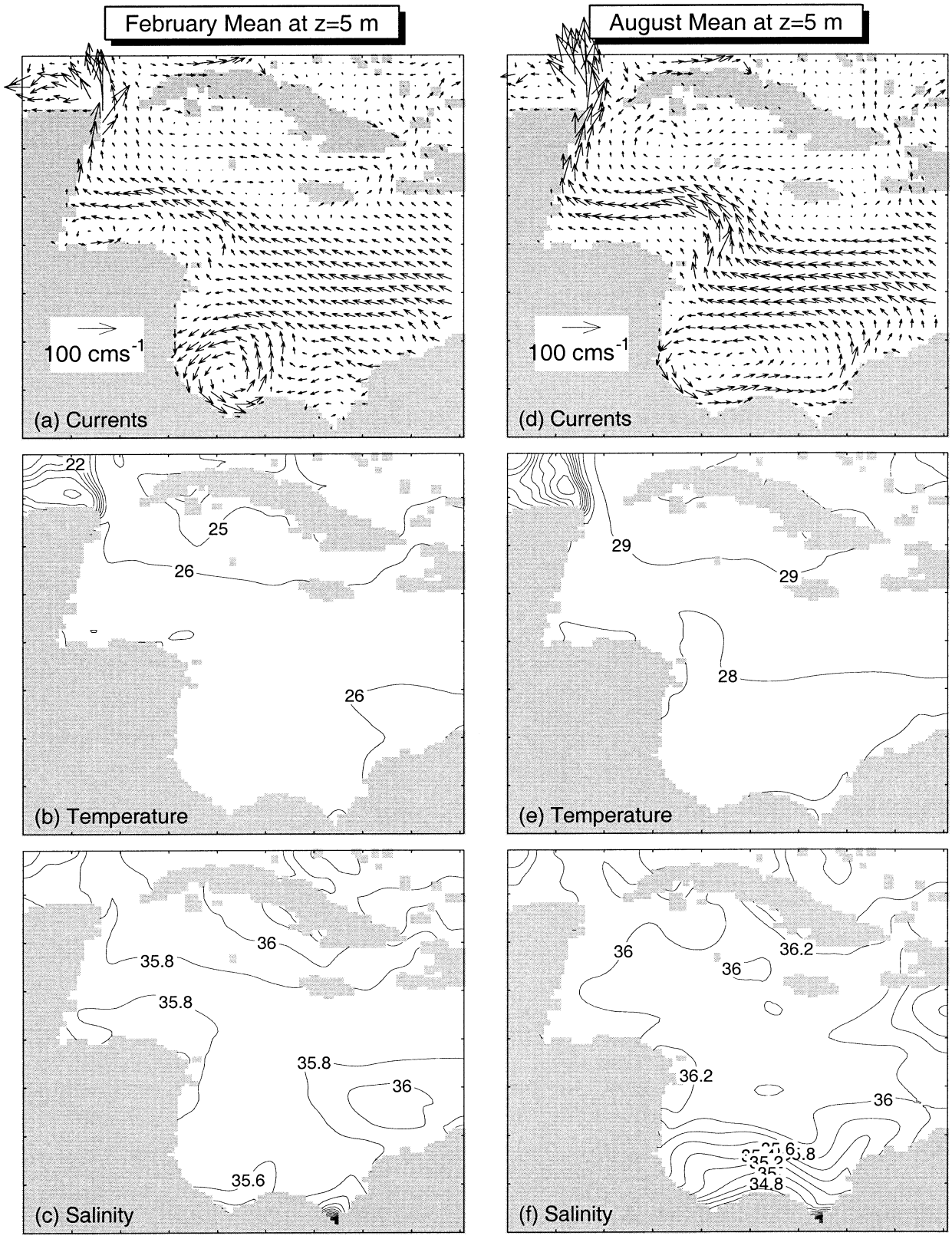

FIG. 9. Monthly mean near-surface (5 m) currents, temperature, and salinity in (left) Feb and (right) Aug, calculated from the 10-yr model results in the control run. Contour intervals are 1°C for temperature and 0.2 ppt for salinity. Velocity vectors are plotted at every third model grid point.

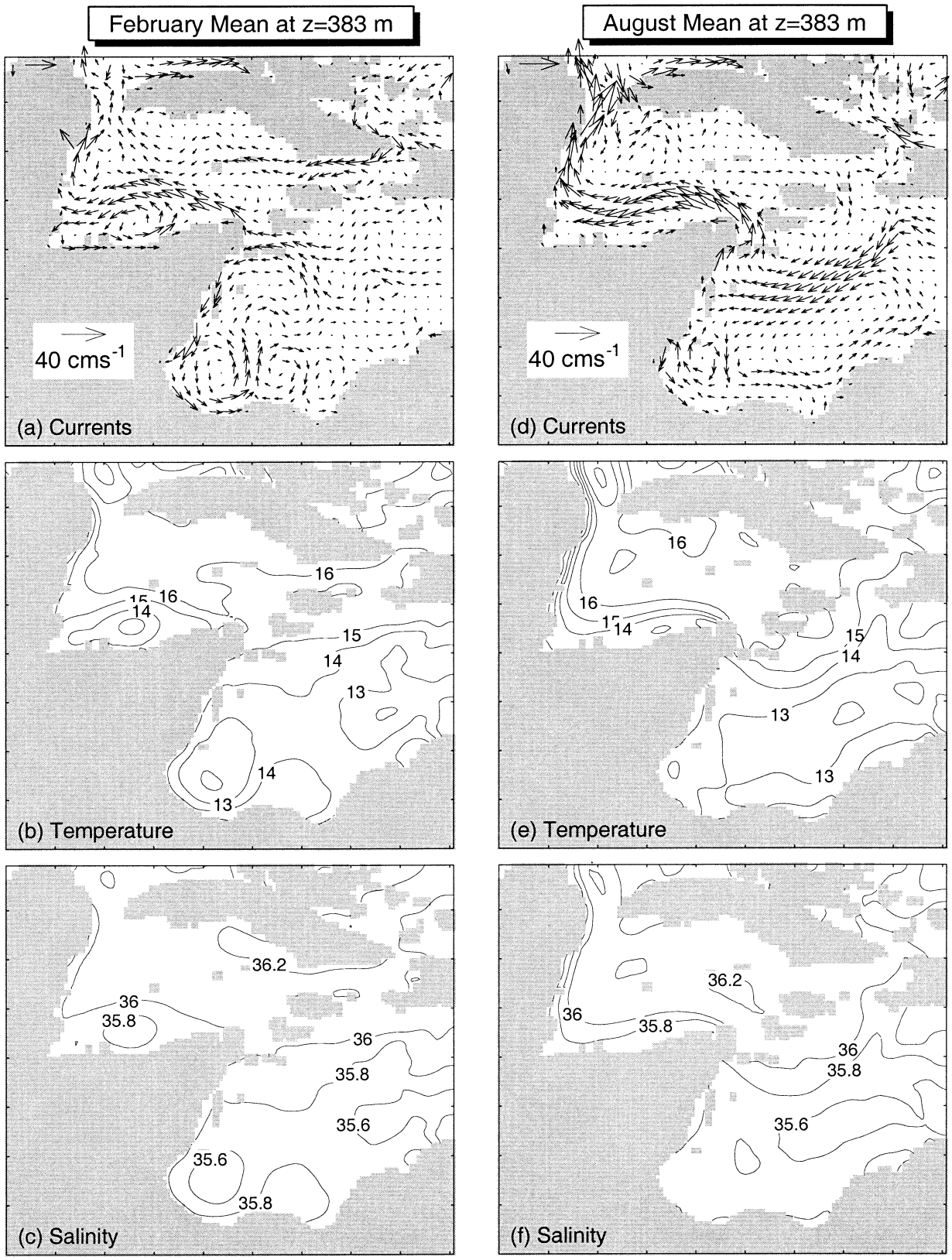

FIG. 10. Monthly mean subsurface (383 m) currents, temperature, and salinity in (left) Feb and (right) Aug, calculated from the 10-yr model results in the control run. Contour intervals and velocity vectors are as for Fig. 9.

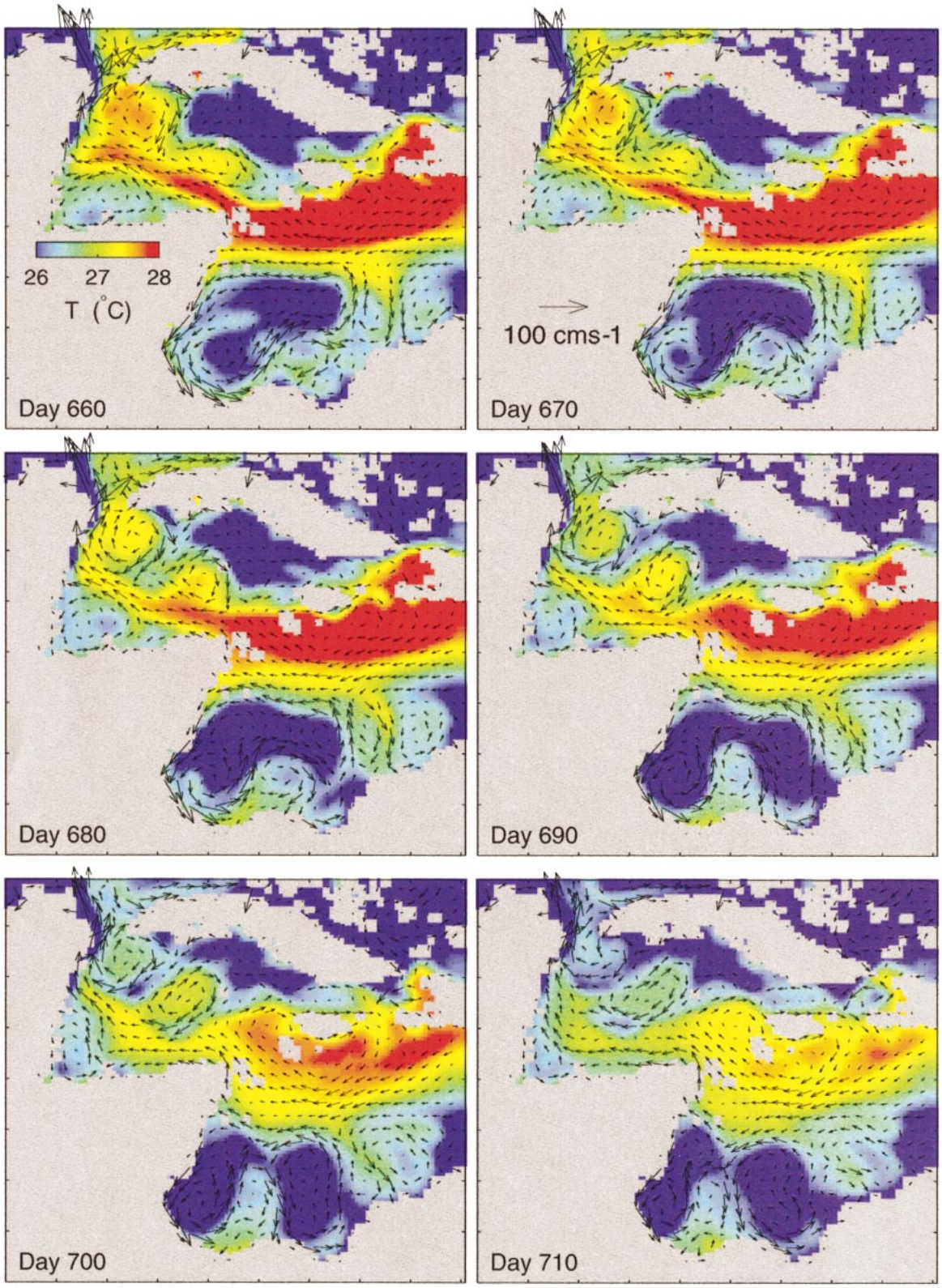

FIG. 11. Snapshots of instantaneous temperature (color image) and currents (arrows) at 80 m during the period of days 660–710 (30 Oct–20 Dec of the second year) in the control run. Time interval is 10 days.

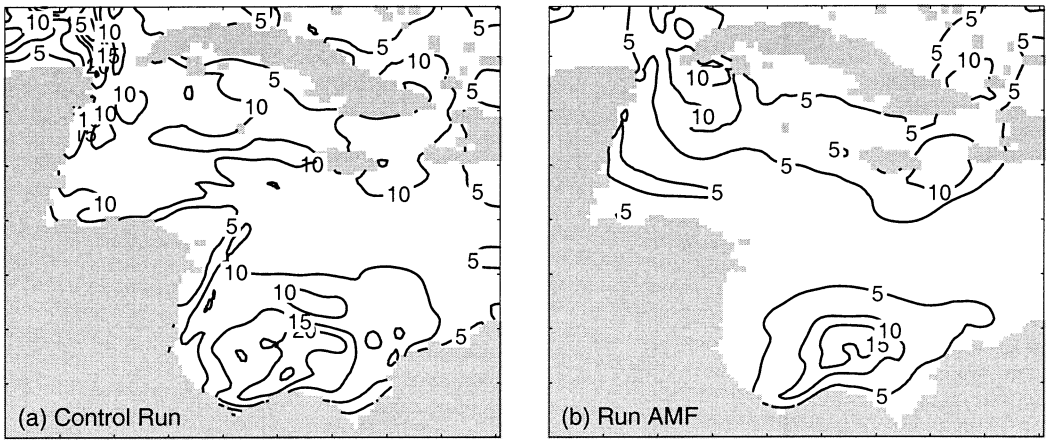

FIG. 12. Vertically averaged rms values of the monthly mean currents relative to the annual mean ($\langle\sigma_s^{|u|}\rangle$) in the top 90 m, calculated from the second-year model simulation. The model is driven by (a) monthly mean forcing (the control run) and (b) AMF.

$$\langle\sigma^u_{(e,s)}\rangle = \frac{1}{z_2 - z_1}\int_{z_2}^{z_1} \sigma^u_{(e,s)}\, dz, \tag{4}$$

where $z_1 = -90$ m and $z_2 = 0$ for the upper ocean and $z_1 = -H$ and $z_2 = -90$ m for the lower ocean, where H is the local water depth. Similarly, we also compute the vertically averaged rms values of $\langle\sigma^T_{(e,s)}\rangle$ and $\langle\sigma^S_{(e,s)}\rangle$ from the second-year model results of temperature and salinity fields. For simplicity, we only consider the value of $\langle\sigma^{|u|}_{(e,s)}\rangle$ in this paper, which is defined as $\sqrt{\langle\sigma^u_{(e,s)}\rangle^2 + \langle\sigma^v_{(e,s)}\rangle^2}$.

The upper-ocean $\langle\sigma_s^{|u|}\rangle$ in the control run are relatively small over the northern Colombian Basin but considerably large over the western Cayman and Yucatan Basins (Fig. 12a), indicating that month-to-month variability of the Caribbean Current is relatively weak in the upper ocean over the Colombian Basin but strong after passing the Nicaragua Rise. The upper-ocean $\langle\sigma_s^{|u|}\rangle$ are also relatively large in the southwestern Colombian Basin, associated mainly with large month-to-month variability of the Panama–Colombia Gyre. The domain-averaged value of $\langle\sigma_s^{|u|}\rangle$ in the control run is about 9.14 cm s^{-1} for the upper ocean (Table 3) and 3.91 cm s^{-1} for the lower ocean, which is about 40% of the upper-ocean value. The domain-averaged values of $\langle\sigma_s^T\rangle$ in the control run are 0.77° and 0.32°C for the upper and lower oceans, respectively. The domain averaged values of $\langle\sigma_s^S\rangle$ are about 0.12 ppt for the upper ocean and about 0.04 ppt for the lower ocean. In comparison with the upper-ocean results, the month-to-month variability of temperature and salinity in the lower ocean is relatively small but not negligible.

To examine correlations between the seasonal variability of the model forcing and month-to-month variability of the model results, we conduct five additional numerical experiments using different combinations of monthly mean and annual mean wind stress, boundary flows, and surface heat and freshwater fluxes (Table 2). These five experiments are model simulations driven respectively by (a) the annual mean (time invariant) forcing in run AMF, and annual mean forcing except for (b) the monthly varying wind stress in run MWS, (c) monthly varying boundary transport in run MBT, (d) monthly varying surface heat fluxes in run MHF, and (e) monthly varying surface freshwater fluxes in run MSF. The model parameters in these five experiments are the same as those in the control run.

Since the model forcing in run AMF is time invariant and the model drift is relatively small with the use of the semiprognostic method, any significant nonzero values of $\langle\sigma_s^{|u|}\rangle$ in this run result primarily from the nonlinear dynamics. The upper-ocean $\langle\sigma_s^{|u|}\rangle$ in this run are

TABLE 3. Vertically averaged rms values of the monthly mean currents ($\langle\sigma_s^{|u|}\rangle$), temperature ($\langle\sigma_s^T\rangle$), and salinity ($\langle\sigma_s^S\rangle$) with respect to the annual means in the upper ocean (depths less than 90 m: upper) and lower ocean (depths greater than 90 m: lower), calculated from the second-year model simulations.

	$\langle\sigma_s^{\|u\|}\rangle$ (cm s^{-1})		$\langle\sigma_s^T\rangle$ (°C)		$\langle\sigma_s^S\rangle$ (ppt)	
Model run	Upper	Lower	Upper	Lower	Upper	Lower
CR	9.14	3.91	0.77	0.32	0.12	0.04
AMF	4.65	1.92	0.09	0.16	0.03	0.02
MWS	5.89	2.06	0.15	0.18	0.04	0.02
MBT	5.96	2.38	0.14	0.20	0.03	0.02
MHF	4.95	1.91	0.63	0.17	0.03	0.02
MSF	4.25	1.83	0.10	0.16	0.07	0.02

relatively small along the pathway of the Caribbean Current, but large in the southwestern Colombian Basin and eastern Cayman and Yucatan Basins (Fig. 12b). The domain-averaged values of $\langle \sigma_s^{|u|} \rangle$ are about 4.65 and 1.92 cm s^{-1}, respectively, for the upper and lower oceans (Table 3), which are about 50% of the values in the control run, indicating that a significant portion of the month-to-month variability of the upper-ocean circulation is accounted for by the nonlinear dynamics. In contrast, the domain-averaged upper-ocean values of $\langle \sigma_s^T \rangle$ and $\langle \sigma_s^S \rangle$ in run AMF are about 0.09°C and 0.03 ppt, respectively (Table 3), which are about 12% and 25% of the values in the control run. Hence, the nonlinear dynamics plays a minor role in simulating month-to-month variability of the upper-ocean temperature and salinity in the control run.

The overall features of the upper-ocean distributions of $\langle \sigma_s^{|u|} \rangle$ in runs MWS and MBT are qualitatively similar to those in run AMF. Main differences occur in the southern Colombian Basin and eastern Cayman and Yucatan Basins, where the upper-ocean rms values of the currents in runs MWS and MBT are relatively larger than those in run AMF, indicating the importance of the monthly varying wind stress and boundary transport in simulating the month-to-month variability of the Panama–Colombia Gyre in the southwestern CS and circulation in the shelf region of western Cuba. The domain-averaged upper-ocean $\langle \sigma_s^{|u|} \rangle$ and $\langle \sigma_s^S \rangle$ are about 6 cm s^{-1} and 0.04 ppt in the two runs (Table 3), which are about 27% and 33% larger than the values in run AMF. The domain-averaged upper-ocean value of $\langle \sigma_s^T \rangle$ in these two runs, on the other hand, is about 0.15°C, which is larger than the value in run AMF but only about 19% of the value in the control run. The domain-averaged rms values of the lower-ocean temperature and salinity in runs MWS and MBT are highly comparable with the values in run AMF. Therefore, the month-to-month variability of the lower-ocean temperature and salinity, on average, is not strongly correlated with the seasonal variability of the wind stress and boundary transports in the region.

Similarly, the upper-ocean distributions of $\langle \sigma_s^{|u|} \rangle$ in runs MHF and MSF have large-scale features very similar to those in run AMF. The domain-averaged upper-ocean values of $\langle \sigma_s^{|u|} \rangle$ are about 5.0 cm s^{-1} in run MHF and 4.3 cm s^{-1} in run MSF (Table 3). The former is only slightly larger than the value in run AMF. The latter is actually smaller than the value in run AMF. Therefore, the month-to-month variability of the upper-ocean circulation in this run is not correlated strongly with the seasonal variability of the surface heat and freshwater fluxes. Reasons for the reduced month-to-month variability of the upper-ocean circulation in run MSF are not clear, although contributing factors could include the restoring boundary conditions used for the surface freshwater fluxes (Pierce 1996). By contrast, the domain-averaged upper-ocean value of $\langle \sigma_s^T \rangle$ in run MHF is about 0.63°C, which is about 7 times the value in run AMF (Table 3 and Fig. 12b) and about 70% of the value in the control run. Therefore, the monthly varying surface heat fluxes play a dominant important role in simulating the seasonal cycle of the upper-ocean temperature. Similarly, the monthly varying surface salinity fluxes play a very important role in simulating the seasonal cycle of the upper-ocean salinity.

The domain-averaged upper-ocean values of $\langle \sigma_e^{|u|} \rangle$ and $\langle \sigma_e^T \rangle$ shown in Fig. 13 are proxies of the mesoscale variability of the model currents and temperature in the upper ocean of less than 90 m. The domain-averaged values of upper-ocean $\langle \sigma_e^{|u|} \rangle$ and $\langle \sigma_e^T \rangle$ are about 4.6 cm s^{-1} and 0.16°C in the control run and about 2.7 cm s^{-1} and 0.06°C in run AMF (Fig. 13), indicating that the nonlinear dynamics, on average, account for more than 60% and 40% of the mesoscale variability for the upper-ocean currents and temperature in the control run. Significant upper-ocean mesoscale variability in the control run occurs in the southwestern CS, western Yucatan Basin and Yucatan Channel, and areas around the Windward Passage. In the northern Colombian Basin, the upper-ocean mesoscale variability is relatively weak. In run AMF, the mesoscale variability of the upper-ocean circulation has large-scale spatial features highly comparable to those in the control run. The domain-averaged upper-ocean values of $\langle \sigma_e^{|u|} \rangle$ are about 4.0 cm s^{-1} in runs MWS, MBT, and MHF and 2.5 cm s^{-1} in run MSF (Fig. 13a). The domain-averaged upper-ocean values of $\langle \sigma_e^T \rangle$ are about 0.07°C in runs MWS, MBT, and MSF and 0.13°C in run MHF (Fig. 13b). Therefore, the upper-ocean mesoscale variability in the control run is largely accounted for by the nonlinear dynamics and partially by monthly varying wind stress, boundary transports, and surface heat fluxes. The mesoscale variability in the upper-ocean temperature is mainly accounted for by the monthly varying surface heat fluxes.

5. Sensitivity study

We conduct three additional numerical experiments to examine the sensitivity of the model results to the linear combination coefficient α of the semiprognostic method and boundary flows specified along the model eastern boundary.

In the first experiment the WCS model is driven by the external forcings in the same way as in the control run (Table 2), except for $\alpha = 0$. This is the case of the pure-prognostic calculation (PP run). We run the model for 11 yr and calculate the time-mean fields from the last 10 yr of model results, as before. The 10-yr mean volume transport streamfunction in the PP run has overall features qualitatively similar to that in the semiprognostic (SP) run (Figs. 5a,c). There are considerable differences, however, in the small-scale features between the two runs, particularly over the southern Colombian Basin and eastern Cayman basin. The February mean subsurface circulation at 383 m in the PP run (Fig. 14) has a much weaker northwestward jet after passing

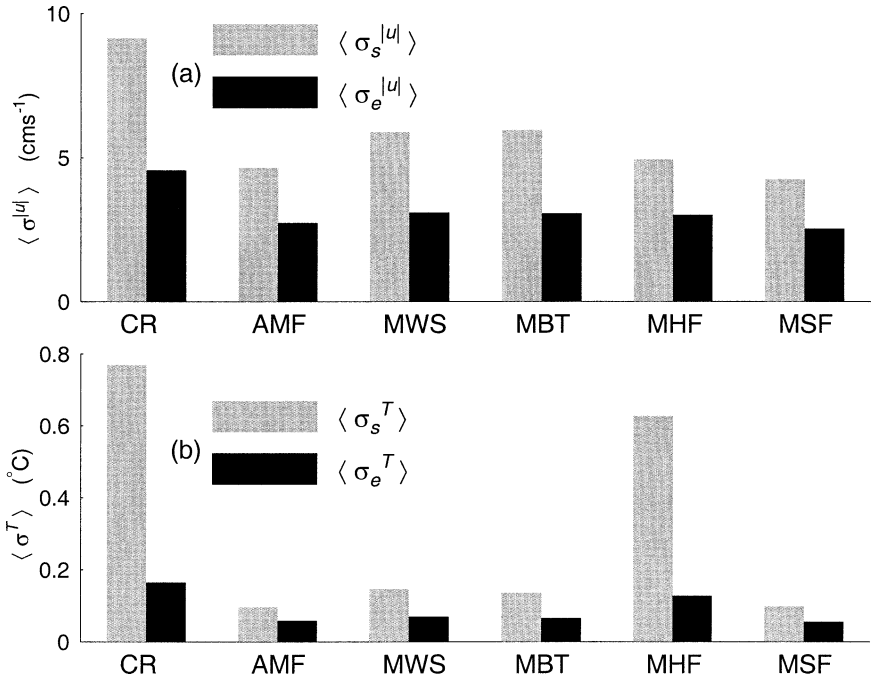

FIG. 13. The domain-averaged upper-ocean values of (a) $\langle \sigma_s^{|u|} \rangle$ and $\langle \sigma_e^{|u|} \rangle$ and (b) $\langle \sigma_s^{T} \rangle$ and $\langle \sigma_e^{T} \rangle$ in the six model runs (see Table 2 for abbreviations of different model runs).

the channel between Nicaragua Rise and Jamaica, in comparison with the subsurface SP results (Fig. 10). The February and August mean subsurface currents of the PP run also differ from the SP results over the Colombian Basin. A comparison of Figs. 2 and 14 indicates that the subsurface temperature and salinity fields of the PP run drift away significantly from the monthly mean climatology.

In the second experiment the WCS model is driven by the external forcings in the same way as in the control run, except for a different depth-mean flow specified along the model eastern open boundary. The depth-mean flow at the eastern boundary in this experiment is the monthly mean flow calculated by the FLAME North Atlantic model without the addition of the uniform westward flow of 0.2 cm s^{-1}. The overall features of the time-mean transport streamfunction in this experiment (Fig. 15a) are highly comparable to the control run (Fig. 5a). The time-mean westward transport of the Caribbean Current is about 17 Sv over the eastern Colombian Basin, and the westward flow through the Windward Passage has a time-mean transport of about 3 Sv. As a result, the mean transport through the Yucatan Strait is about 20 Sv, which is about 20% smaller than that in the control run. The model-calculated currents, temperature and salinity in this experiment are highly comparable to the control run.

The WCS model in the third experiment is forced in the same way as in the control run, except that the FLAME model results and the uniform westward flow at the eastern open boundary are not used. The 10-yr mean volume transport streamfunction in this experiment (Fig. 15b) differs significantly from the control run, indicating the importance of the FLAME model results in driving the WCS model.

6. Summary

The primitive equation z-level ocean circulation model known as CANDIE was applied to the western Caribbean Sea. The model was forced with the climatological monthly mean forcing including wind stress, surface heat and freshwater fluxes, and flows across the model open boundary. The semiprognostic method (Sheng et al. 2001) was used to reduce the model drift. The limited-area WCS model was integrated for 11 yr and the time-mean fields were calculated from the model results during the last 10 yr. The 10-yr mean volume transports produced by the model are in good agreement with the latest estimates by Johns et al. (2002), with about 19 and 7 Sv westward transports through the Beata Transect and Windward Passage and a 26 Sv northward transport through the Yucatan Strait. Sheinbaum et al. (2002) recently suggested that the time mean volume transport across the Yucatan Strait is only about 23.8 $\pm$ 1 Sv, based on the direct current observations from September 1999 to June 2000. Their transport estimate is about 10% smaller than the other estimates. Future studies are needed to determine whether their low transport estimate reflects interannual variability of the currents through the strait, or indicates the overestimation of the mean transport made by previous studies.

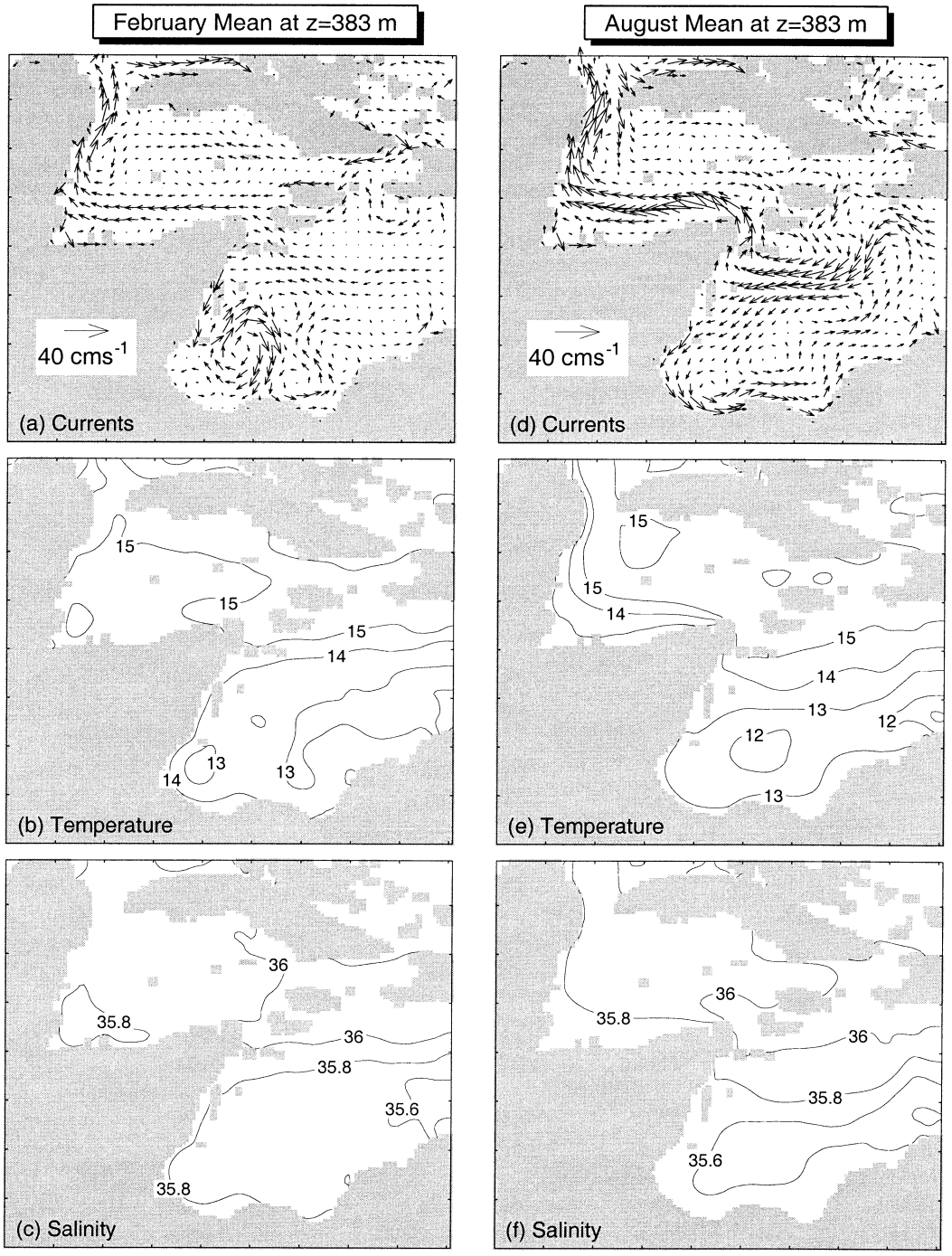

FIG. 14. As in Fig. 10, but for pure-prognostic results.

The model-calculated 10-yr mean currents in the WCS are characterized by the relatively persistent, surface-intensified throughflow known as the Caribbean Current over the northern Colombian Basin and western Cayman and Yucatan Basins and the highly variable Panama–Colombia Gyre. The mean circulation over the eastern Cayman and Yucatan Basins is relative weak in the upper ocean of less than 90 m, with relatively stronger westward flow in the lower ocean as a result of the inflow running through the Windward Passage. The model-calculated 10-yr mean circulation is in good agreement with the observed currents inferred from the trajectories of 15-m drogued, satellite-tracked drifters (Fratantoni 2001) in the study region. The model-calculated currents along the Yucatan Strait also agree well with the direct current measurements (Sheinbaum et al.

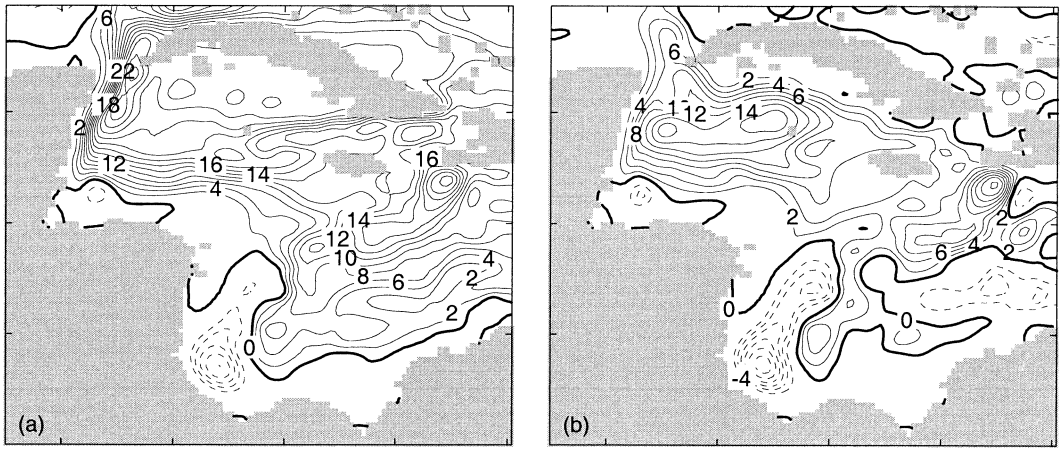

FIG. 15. Time-mean volume transport streamfunction calculated from the 10-yr model results. The model is driven by the external forcings in the same way as in the control run (Fig. 5a), except for different depth-mean flows specified at the eastern open boundary. (a) The depth-mean flow at the eastern boundary is the monthly mean FLAME results without the addition of the uniform westward flow of 0.2 cm s^{-1}. (b) Both the FLAME results and uniform westward flow are not used.

2002). It should be noted that the model–data comparisons made in this paper are qualitative to some extent. Quantitative comparisons can be made by driving the ocean model with synoptic sea surface and lateral open boundary forcings, which is beyond the scope of this study.

The WCS model was also used to determine the main dynamics responsible for the month-to-month and mesoscale variability in the model results. The nonlinear dynamics, monthly varying wind stress, and flows across the model eastern boundary all play a very important role in simulating the month-to-month and mesoscale circulation variability in the region. The monthly varying surface heat fluxes are largely responsible for the seasonal cycle of the temperature in the upper ocean. The model results, however, underestimate the mesoscale variability in the northern Colombian Basin, mainly because of the specification of monthly mean flows across the eastern open boundary.

Acknowledgments. We thank Richard Greatbatch, Bruce Hatcher, and Barry Ruddick for their useful suggestions and comments. We thank David Fratantoni for providing the near-surface currents determined from the 15-m drogued satellite-tracked drifters in the North Atlantic, Julio Sheinbaum for providing the time-mean observed currents and temperature across Yucatan Strait, and Carsten Eden for providing monthly mean transports in the North Atlantic produced by FLAME. This project is part of the ECONAR (Ecological Connections Among Reefs) supported by the Collaborative Research Opportunity Program of the Natural Sciences and Engineering Research Council of Canada (NSERC). Author JS is also supported by NSERC, MARTEC (a Halifax-based company), and the Meteorological Service of Canada (MSC) through the NSERC/MARTEC/MSC Industrial Research Chair in ''Regional Ocean Modelling and Prediction.''

APPENDIX

Basic Equations of the Ocean Circulation Model

The three-dimensional primitive equation ocean circulation model known as CANDIE (see online at http://www.phys.ocean.dal.ca/programs/CANDIE, or see Sheng et al. 1998, 2001) is used in this study. The governing equations of the model can be written in spherical coordinates as

$$\frac{\partial u}{\partial t} + \mathcal{L}u - \left(f + \frac{u\tan\phi}{R}\right)v = -\frac{1}{\rho_o R\cos\phi}\frac{\partial p}{\partial \lambda} + \mathcal{D}_m u + \frac{\partial}{\partial z}\left(K_m\frac{\partial u}{\partial z}\right), \quad \text{(A1)}$$

$$\frac{\partial v}{\partial t} + \mathcal{L}v + \left(f + \frac{u\tan\phi}{R}\right)u = -\frac{1}{\rho_o R}\frac{\partial p}{\partial \phi} + \mathcal{D}_m v + \frac{\partial}{\partial z}\left(K_m\frac{\partial v}{\partial z}\right), \quad \text{(A2)}$$

$$\frac{1}{R\cos\phi}\left[\frac{\partial u}{\partial \lambda} + \frac{\partial(v\cos\phi)}{\partial\phi}\right] + \frac{\partial w}{\partial z} = 0, \quad \text{(A3)}$$

$$\frac{\partial p}{\partial z} = -[\alpha\rho_m + (1-\alpha)\rho_c]g, \quad \text{(A4)}$$

$$\rho_m = \rho(T, S, p_r), \quad \text{(A5)}$$

$$\rho_c = \rho(T_c, S_c, p_r), \quad \text{(A6)}$$

$$\frac{\partial T}{\partial t} + \mathcal{L}T = \mathcal{D}_h T + \frac{\partial}{\partial z}\left(K_h \frac{\partial T}{\partial z}\right), \quad \text{and} \tag{A7}$$

$$\frac{\partial S}{\partial t} + \mathcal{L}S = \mathcal{D}_h S + \frac{\partial}{\partial z}\left(K_h \frac{\partial S}{\partial z}\right), \tag{A8}$$

where u, v, w are the east (λ), north (ϕ), and vertical (z) components of the flow; p is pressure (see below); and ρ_m is the density calculated from the model potential temperature T and salinity S, which in turn, are updated using the conservation equations defined in Eqs. (A7) and (A8). Here ρ_c is the density calculated from climatological potential temperature T_c and salinity S_c, p_r is the reference pressure at the center of each z level, K_m and K_h are vertical eddy viscosity and diffusivity coefficients, f is the Coriolis parameter, ρ_o is a reference density, R and g are the earth's radius and gravitational acceleration, $\mathcal{L}$ is an advection operator defined as

$$\mathcal{L}q = \frac{1}{R\cos\phi}\frac{\partial(uq)}{\partial\lambda} + \frac{1}{R\cos\phi}\frac{\partial(vq\cos\phi)}{\partial\phi} + \frac{\partial(wq)}{\partial z}, \tag{A9}$$

and $\mathcal{D}_m$ and $\mathcal{D}_h$ are diffusion operators defined as

$$\mathcal{D}_{(m,h)}q = \frac{1}{R^2}\left\{\frac{1}{\cos^2\phi}\frac{\partial}{\partial\lambda}\left[A_{(m,h)}\frac{\partial q}{\partial\lambda}\right] + \frac{\partial q}{\partial\phi}\left[\cos\phi A_{(m,h)}\frac{\partial q}{\partial\phi}\right]\right\}, \tag{A10}$$

where A_m and A_h are horizontal eddy viscosity and diffusivity coefficients, respectively.

The model uses the subgrid-scale mixing parameterization scheme of Smagorinsky (1963) for the horizontal eddy viscosity A_m and the schemes proposed by Large et al. (1994) for the vertical mixing coefficients K_m and K_h. The turbulent Prandtl number A_h/A_m is set to 0.1. The model also uses the fourth-order numerics (Dietrich 1997) and Thuburn's flux limiter to discretize the nonlinear advection terms (Thuburn 1996).

The governing equations presented above are conventional, except for the terms in square brackets on the right side of the hydrostatic equation, Eq. (A4). Here the conventional density term is replaced by a linear combination of model-computed density (ρ_m) and climatological density (ρ_c): $\alpha\rho_m + (1 - \alpha)\rho_c = \rho_m + (1 - \alpha)(\rho_c - \rho_m)$, where α is the linear combination coefficient with a value between 0 and 1, which is the semiprognostic method suggested by Sheng et al. (2001). The ocean circulation model is purely prognostic if $\alpha = 1$ and purely diagnostic if $\alpha = 0$.

As discussed in Sheng et al. (2001), the semiprognostic method is used to adiabatically adjust the momentum equations of an ocean circulation model to correct for the model errors associated with the physical processes that are not correctly represented by the model equations, leaving the temperature and salinity equations unconstrained and fully prognostic. To demonstrate this we separate the pressure variable p into two parts

$$p = p^* + \tilde{p}, \tag{A11}$$

where

$$\frac{\partial p^*}{\partial z} = -\rho_m g \quad \text{and} \tag{A12}$$

$$\frac{\partial \tilde{p}}{\partial z} = -(1 - \alpha)(\rho_c - \rho_m)g. \tag{A13}$$

Writing the horizontal momentum equations in terms of p^* and $\tilde{p}$, we obtain

$$\frac{\partial u}{\partial t} = -\frac{1}{\rho_o R\cos\phi}\frac{\partial p^*}{\partial\lambda} - \frac{1}{\rho_o R\cos\phi}\frac{\partial\tilde{p}}{\partial\lambda} + \text{others}, \tag{A14}$$

and

$$\frac{\partial v}{\partial t} = -\frac{1}{\rho_o R}\frac{\partial p^*}{\partial\phi} - \frac{1}{\rho_o R}\frac{\partial\tilde{p}}{\partial\phi} + \text{others}. \tag{A15}$$

It can be seen that p^* corresponds to the traditional pressure variable carried by the model, since p^* satisfies the conventional hydrostatic equation and surface boundary condition. On the other hand, the terms involving $\tilde{p}$ appear as forcing terms in the model momentum equations, and it is these forcing terms that are responsible for modifying the model-computed velocities that, in turn, modify the tracers through the advection terms in Eqs. (A7) and (A8). The forcing terms associated with $\tilde{p}$ can be thought of as representing unresolved processes.

REFERENCES

Andrade, C. A., and E. D. Barton, 2000: Eddy development and motion in the Caribbean Sea. *J. Geophys. Res.*, **105,** 26 191–26 201.

Daley, R., 1991: *Atmospheric Data Analysis.* Cambridge University Press, 457 pp.

da Silva, A. M., C. C. Young, and S. Levitus, 1994: *Anomalies of Heat and Momentum Fluxes.* Vol. 3, *Atlas of Surface Marine Data 1994*, NOAA Atlas NESDIS 8, 413 pp.

Davidson, F., R. J. Greatbatch, and B. deYoung, 2001: Asymmetry in the response of a stratified coastal embayment to wind forcing. *J. Geophys. Res.*, **106,** 7001–7016.

Dengg, J., C. Boening, U. Ernst, R. Redler, and A. Beckmann, 1999: Effects of an improved model representation of overflow water on the subpolar North Atlantic. *International WOCE Newsletter*, No. 37, WOCE International Project Office, Southampton, United Kingdom, 10–15.

Dietrich, D. E., 1997: Application of a modified Arakawa 'a' grid ocean model having reduced numerical dispersion to the Gulf of Mexico circulation. *Dyn. Atmos. Oceans*, **27,** 201–217.

——, M. G. Marietta, and P. J. Roache, 1987: An ocean modelling system with turbulent boundary layers and topography: Numerical description. *Int. J. Numer. Methods Fluids*, **7,** 833–855.

Fratantoni, D. F., 2001: North Atlantic surface circulation during the 1990's observed with satellite-tracked drifters. *J. Geophys. Res.*, **106,** 22 067–22 093.

Gallegos, A., 1996: Descriptive physical oceanography of the Caribbean Sea. *Small Islands: Marine Science and Sustainable De-*

velopment, G. A. Maul, Ed., Vol. 51, *Coastal and Estuarine Studies*, Amer. Geophys. Union, 36–55.
Gordon, A. L., 1967: Circulation of the Caribbean Sea. *J. Geophys. Res.*, **72,** 6207–6223.
Haney, R. L., 1971: Surface thermal boundary conditions for ocean circulation models. *J. Phys. Oceanogr.*, **1,** 241–248.
Hellerman, S., and M. Rosenstein, 1983: Normal monthly wind stress over the world ocean with error estimates. *J. Phys. Oceanogr.*, **13,** 1093–1104.
Hurlburt, H. E., and T. L. Townsend, 1994: NRL effort in the North Atlantic. *Data Assimilation and Model Evaluation Experiments: North Atlantic Basin Preliminary Experiment Plan*, R. C. Willems, Ed., Tech. Rep. TR-2/95, University of Southern Mississippi, 30–35.
Johns, W. E., T. L. Townsend, D. M. Fratantoni, and W. D. Wilson, 2002: On the Atlantic inflow to the Caribbean Sea. *Deep-Sea Res.*, **49A,** 211–243.
Kinder, T. H., G. W. Huburn, and A. W. Green, 1985: Some aspects of the Caribbean circulation. *Mar. Geol.*, **68,** 25–52.
Large, W. G., J. C. McWilliams, and S. C. Doney, 1994: Oceanic vertical mixing: A review and a model with a nonlocal boundary layer parameterization. *Rev. Geophys.*, **32,** 363–403.
Lu, Y., K. R. Thompson, and D. G. Wright, 2001: Tidal currents and mixing in the Gulf of St. Lawrence: An application of the incremental approach to data assimilation. *Can. J. Fish. Aquat. Sci.*, **58,** 723–735.
Marchesiello, P., J. C. WcWilliams, and A. Shchepetkin, 2001: Open boundary conditions for long-term integration of regional oceanic models. *Ocean Modell.*, **3,** 1–20.
Maul, G. A., Ed., 1993: *Climatic Change in the Intra-Americas Sea*. Edward Arnold, 389 pp.
Model, F., 1950: Pillsbury's Strommessungen und der Wasserhaushalt des Amerikanischen Mittelmeeres. *Dtsch. Hydrogr. Z.*, **3,** 57–61.
Mooers, C. N. K., and G. A. Maul, 1998: Intra-Americas sea circulation, coastal segment(3,W). *The Sea*, A. Robinson and K. H. Brink, Eds., Vol. 11, John Wiley and Sons, 183–208.
Muller-Karger, F. E., 1993: River discharge variability including satellite-observed plume-dispersal patterns. *Climate Change in the Intra-Americas Sea*, G. A. Maul, Ed., Edward Arnold, 162–192.
Murphy, S. J., H. E. Hurlburt, and J. J. O'Brien, 1999: The connectivity of eddy variability in the Caribbean Sea, the Gulf of Mexico, and the Atlantic Ocean. *J. Geophys. Res.*, **104,** 1431–1453.
Nystuen, J. A., and C. A. Andrade, 1993: Tracking mesoscale ocean features in the Caribbean Sea using *Geosat* altimetry. *J. Geophys. Res.*, **98,** 8389–8394.
Orlanski, I., 1976: A simple boundary condition for unbounded hyperbolic flows. *J. Comput. Phys.*, **21,** 251–269.
Pierce, D. W., 1996: Reducing phase and amplitude errors in restoring boundary conditions. *J. Phys. Oceanogr.*, **26,** 1552–1560.
Roemmich, D., 1981: Circulation of the Caribbean Sea: A well-resolved inverse problem. *J. Geophys. Res.*, **86,** 7993–8005.
Ruiz Renteria, F. G., 1979: Upwelling north of the Yucatan Peninsula. M.S. thesis, Dept. of Oceanography, Texas A&M University, 92 pp.
Schmitz, W., and P. L. Richardson, 1991: On the sources of the Florida Current. *Deep-Sea Res.*, **38,** S379–S409.
Sheinbaum, J., J. Candela, A. Badan, and J. Ochoa, 2002: Flow structure and transport in the Yucatan Channel. *Geophys. Res. Lett.*, **29,** 1040, doi:10.1029/2001GL013990.
Sheng, J., 2001: Dynamics of a buoyancy-driven coastal jet: The Gaspé Current. *J. Phys. Oceanogr.*, **31,** 3146–3163.
——, D. G. Wright, R. J. Greatbatch, and D. E. Dietrich, 1998: CANDIE: A new version of the DieCAST ocean circulation model. *J. Atmos. Oceanic Technol.*, **15,** 1414–1432.
——, R. J. Greatbatch, and D. G. Wright, 2001: Improving the utility of ocean circulation models through adjustment of the momentum balance. *J. Geophys. Res.*, **106,** 16 711–16 728.
Smagorinsky, J., 1963: General circulation experiments with the primitive equation. I. The basic experiment. *Mon. Wea. Rev.*, **91,** 99–164.
Smith, R. D., M. E. Maltrud, F. O. Bryan, and M. W. Hecht, 2000: Numerical simulation of the North Atlantic Ocean at 1/10°. *J. Phys. Oceanogr.*, **30,** 1532–1561.
Thuburn, J., 1996: Multidimensional flux-limited advection schemes. *J. Comput. Phys.*, **123,** 74–83.
Worthington, L., 1976: *On the North Atlantic Circulation.* Johns Hopkins Press, 110 pp.
Wunsch, C., and B. Grant, 1982: Towards the general circulation of the North Atlantic Ocean. *Progress in Oceanography*, Vol. 11, Pergamon, 1–59.
Wust, G., 1964: *Stratification and Circulation in the Antillean–Caribbean Basins. Part I: Spreading and Mixing of the Water Types with an Oceanographic Atlas.* Columbia University Press, 201 pp.